Available online at www.sciencedirect.com
SciVerse ScienceDirect
Journal of the European Ceramic Society 32 (2012) 2557–2563
www.elsevier.com/locate/jeurceramsoc

Microstructure refinement and mechanical properties improvement of HfB_2–SiC composites with the incorporation of HfC

De-Wei Ni, Ji-Xuan Liu, Guo-Jun Zhang *

State Key Laboratory of High Performance Ceramics and Superfine Microstructures, Shanghai Institute of Ceramics, Shanghai 200050, China

Received 11 September 2011; received in revised form 29 January 2012; accepted 12 February 2012
Available online 8 March 2012

Abstract

HfB_2 and HfB_2–10 vol% HfC fine powders were synthesized by carbo/boronthermal reduction of HfO_2, which showed high sinterability. Using the as-synthesized powders and commercially available SiC as starting powders, nearly full dense HfB_2–20 vol% SiC (HS) and HfB_2–8 vol% HfC–20 vol% SiC (HHS) ceramics were obtained by hot pressing at 2000 °C/30 MPa. With the incorporation of HfC, the grain size of HHS was much finer than HS. As well, the fracture toughness and bending strength of HHS (5.09 MPa $m^{1/2}$, 863 MPa) increased significantly compared with HS (3.95 MPa $m^{1/2}$, 654 MPa). Therefore, it could be concluded that the incorporation of HfC refined the microstructure and improved the mechanical properties of HfB_2–SiC ceramics.

Keywords: Hot pressing; Mechanical properties; Hafnium diboride; UHTCs; Synthesis

1. Introduction

As a member of the ultrahigh temperature ceramics (UHTCs) family, transition metal carbides (MC, M = Hf, Zr) has a higher melting temperature and refractory.[1] Accordingly, the addition of MC to MB_2–SiC (one of the main systems of UHTCs) to form a ternary composite of MB_2–SiC–MC might adjust the microstructure and properties of MB_2–SiC composite. Recent years, a variety of research has been carried out on the ZrB_2–SiC–ZrC system, including the densification behavior, microstructures evolution, as well as the fabrication processing and properties.[2–6] Corresponding studies have confirmed that the MB_2–SiC–MC ceramics have superior resistance to ablation than the corresponding MB_2–SiC ceramics under an arc-jet environment.[7] To the best of the author's knowledge, studies on the HfB_2–SiC–HfC system are very limited. Monteverde studied the in situ synthesis of HfB_2–SiC–HfC by reactive hot pressing using Hf metal with B_4C and silicon as starting materials.[8] Licheri et al. studied the densification and microstructures of HfB_2–SiC and HfB_2–HfC–SiC composites by self-propagating high-temperature synthesis (SHS) followed by spark plasma sintering (SPS).[9] In the ZrB_2–SiC–ZrC system, Guo and Zhang pointed out that the addition of ZrC improved the densification and mechanical properties of ZrB_2–SiC ceramics evidently.[6] However, the effect of HfC addition on the microstructure development and the resulted different properties in the HfB_2–SiC system is still not clear.

On the other side, ultrafine powders have been widely demonstrated good sinterability and resulted in superior properties. In our previous study, HfB_2 was synthesized via carbo/borothermal reduction of HfO_2 with B_4C and carbon.[10] Combining the characteristics of carbo/borothermal reduction, HfB_2–HfC composite powders could also be synthesized by adjusting the starting powder ratio via carbo/borothermal reduction route. It is believed that the in situ synthesized HfB_2–HfC powders must lead to much more homogeneous distribution, which is much beneficial for the properties improvement of ceramics.

In this work, we aimed to investigate the effect of HfC on the microstructure and properties of HfB_2–SiC system. HfB_2 and HfB_2–10 vol% HfC powders were synthesized by boro/carbothermal reduction firstly. Then, HfB_2–20 vol% SiC (HS) and HfB_2–8 vol% HfC–20 vol% SiC (HHS) ceramics were

* Corresponding author. Tel.: +86 21 52411080; fax: +86 21 52413122.
E-mail address: gjzhang@mail.sic.ac.cn (G.-J. Zhang).

0955-2219/$ – see front matter © 2012 Elsevier Ltd. All rights reserved.
doi:10.1016/j.jeurceramsoc.2012.02.017

hot pressed using as-synthesized HfB_2, HfB_2–10 vol% HfC and commercially available SiC as starting powders. The densification behavior, microstructure and mechanical properties of the hot pressed ceramics were investigated. The emphasis is put on the effects of HfC on the microstructure development and mechanical properties.

2. Experimental procedure

HfO_2 (purity 99.9%, main impurities include Zr 0.46%, specific surface area by BET about 11.3 m^2/g, particle size < 2 μm for 98%, Found Star Science and Technology Co., Ltd., Beijing, China), B_4C (D_{50} = 1.5 μm, purity 96%, Jingangzuan Boron Carbide Co., Ltd., Mudanjiang, China) and graphite (D_{50} = 1.5 μm, purity 99%, colloid chemistry Co., Ltd., Shanghai, China) were used as starting powders to synthesize HfB_2 and HfB_2–HfC. By adjusting the amounts of HfO_2, B_4C, and carbon in a desired molar ratio, HfB_2 and HfB_2–10 vol% HfC powders were synthesized at 1600 °C in vacuum (∼5 Pa). The details of powder synthesis processing could be found in our previous work.[10]

Commercially available SiC powder (D_{50} = 0.45 μm, purity 98.5%, Changle Xinyuan Carborundum Micropowder Co. Ltd., Changle, China) was added to the synthesized HfB_2 and HfB_2–HfC powders to fabricate HfB_2–20 vol% SiC (HS) and HfB_2–10 vol% HfC–20 vol% SiC (HHS) ceramics, respectively. The starting mixtures were mixed for 24 h in plastic bottles using absolute ethanol and SiC balls as medium, and dried by rotary evaporation at 70 °C. After that, the mixed powders were sieved through a 200-mesh screen and then placed in a graphite die with a BN coating. Subsequently, the composites were hot pressed at 2000 °C for 1 h under a pressure of 30 MPa in an argon atmosphere with a heating rate of 10 °C/min. The hot pressed samples had dimensions of 37 mm × 30 mm × 4 mm.

Phase composition was determined by X-ray diffraction (XRD, D/max 2550 V, Rigaku Corporation, Japan) using Cu K_α radiation (λ = 1.54178 Å). The mass fraction of HfB_2 and HfC in the synthesized HfB_2–HfC powder was estimated based on the relative intensity of the strongest diffraction peak using K value method.[10,11] The mean diameter and particle size distribution of the synthesized powders were analyzed using a laser particle size analysis (Microtrac, Nikkiso Co. Ltd., Tokyo, Japan). The oxygen and carbon content of the as-synthesized powders were determined by nitrogen/oxygen determinator (TC600, LECO, St. Joseph, MI) and carbon determinator, respectively.

After removing the surface layer from the hot-pressed disks, the bulk density was measured using the Archimedes method with distilled water as the immersing medium, while the theoretical density was estimated with the rule of mixture. The microstructure characteristics of polished sections and fracture surfaces were observed by scanning electronic microscopy (SEM). Grain sizes of the as-sintered ceramics were determined with an average of 100 grains using an image analysis software package (Image-Pro). The Vickers' hardness and fracture toughness were determined by the indentation method (Wilson-Wolpert Tukon2100B, Instron, Norwood, MA), using a diamond indenter with a load of 5 kg for 10 s on a polished surface; the reported value was an average of 3 measurements. The fracture toughness was calculated by the following equation[12,13]:

$$K_{IC} = P\left[\pi\left(\frac{C_1 + C_2}{4}\right)\right]^{-(3/2)} (\tan\,\beta)^{-1} \tag{1}$$

where P is the indentation load (N), C_1 and C_2 are the measured diagonal crack length (m), and β is an angle constant (68°). Flexural strength was measured by a 3-point bending test (test bars 3 mm × 4 mm × 36 mm) with a span of 30 mm and the crosshead speed was 0.5 mm/min; the reported strength value was an average of 5 measurements. The Young's modulus (E) was also obtained from the bending test using the following equation:

$$E = \frac{L^3(P_2 - P_1)}{4BH^3(Y_{t2} - Y_{t1})} \tag{2}$$

where P_1 and P_2 are the initial and final load (N) of linear range respectively, L is the span (mm), B and H are the width (mm) and thickness (mm) of samples respectively, Y_{t1} and Y_{t2} are the deflection (mm) when load are P_1 and P_2 respectively.

3. Results and discussion

3.1. Synthesis of HfB_2 and HfB_2–HfC powders

HfB_2 was synthesized based on the following carbo/borothermal reduction reaction:

$$HfO_2 + 0.5B_4C + 1.5C = HfB_2 + 2CO \tag{3}$$

Thermodynamic calculation showed that the above reaction became favorable at ∼1500 °C in the standard state. And it could be reduced to below 1000 °C at $P_{CO} \sim 10$ Pa by thermodynamic calculation. However, previous studies showed that 1500–1600 °C was needed to ensure reaction to completeness. Therefore, 1600 °C was chosen as the reaction temperature in this work. Compared with reaction (3), previous studies have shown that HfO_2 could react with B_4C at lower temperatures:

$$HfO_2 + \tfrac{5}{7}B_4C = HfB_2 + \tfrac{5}{7}CO + \tfrac{3}{7}B_2O_3 \tag{4}$$

At the same time, the produced B_2O_3 would continue to react with HfO_2 and carbon to form HfB_2.

$$HfO_2 + B_2O_3 + 5C = HfB_2 + 5CO \tag{5}$$

If all the produced B_2O_3 reacted with HfO_2 and carbon, the reaction (3) could be derived by combining the above two reactions (4) and (5) with the molar ratio 1:0.5 of HfO_2 and B_4C. However, B_2O_3 had a high vapor pressure and vaporized rapidly above 1100 °C. Accordingly, vaporization of B_2O_3 would induce an excess of HfO_2 and C, which resulted in the formation of HfC based on reaction (6):

$$HfO_2 + 3C = HfC + 2CO \tag{6}$$

Therefore, HfC was presented in the final product synthesized from a stoichiometric ratio of the starting materials according to reaction (3) owing to the vaporization of B_2O_3. And early results showed that the content of HfC was 14.8 wt%. By adjusting

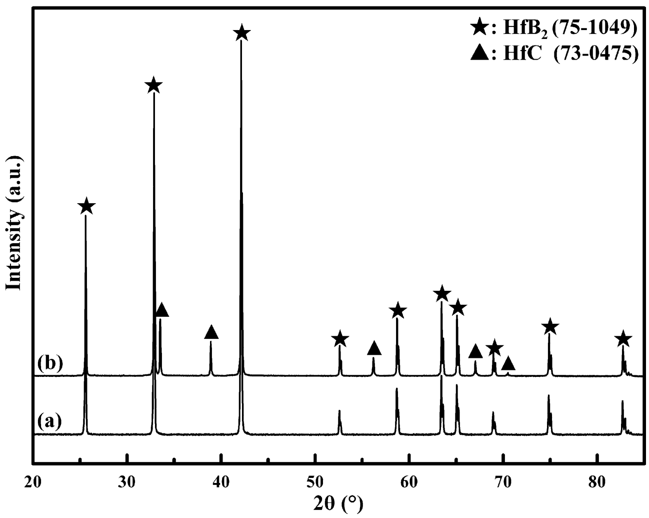

Fig. 1. XRD patterns of the as-synthesized HfB_2 (a) and HfB_2–HfC (b) powders at 1600 °C for 1 h.

the amounts of starting powders HfO_2, B_4C and carbon, the proportion of HfB_2 and HfC could be regulated. In other words, HfB_2 and HfB_2–HfC powders with different HfC content could be obtained by adjusting the amounts of B_4C and C.

At first, we adjusted the amounts of B_4C and C in some sort (mol ratio HfO_2:B_4C:C = 1:0.55:1.4). As shown in Fig. 1(b), the as-synthesized powder was composed of HfB_2 and HfC. The relative intensity of HfC's strongest diffraction peak is about 17.47% for the as-synthesized HfB_2–HfC powder. For HfB_2 and HfC, the reference spectral intensity is 13.14 and 16.99 from PDF cards 75-1049 and 73-0475, respectively. The mass fraction of HfC was estimated to be about 11.2 wt% for the as-synthesized HfB_2–HfC based on the XRD using *K* value method. Therefore, the volume proportion of HfB_2 and HfC was about 90:10 based on the densities of 11.21 and 12.69 g cm^{-3} for HfB_2 and HfC, respectively. Monolithic HfB_2 powder was also synthesized based on previous results. As shown in Fig. 1(a), only hexagonal HfB_2 phase presented in Fig. 1(a) and no evidence of HfO_2, HfC, or other impurities was observed. The oxygen content of the as-synthesized HfB_2 and HfB_2–HfC powders are 0.30 wt% and 0.19 wt%, respectively. The carbon content of HfB_2–HfC powder was about 0.81 wt%, which was a little higher than the calculated results of XRD. And the excessive carbon should be residual graphite or boron carbide, which will be discussed in the following section.

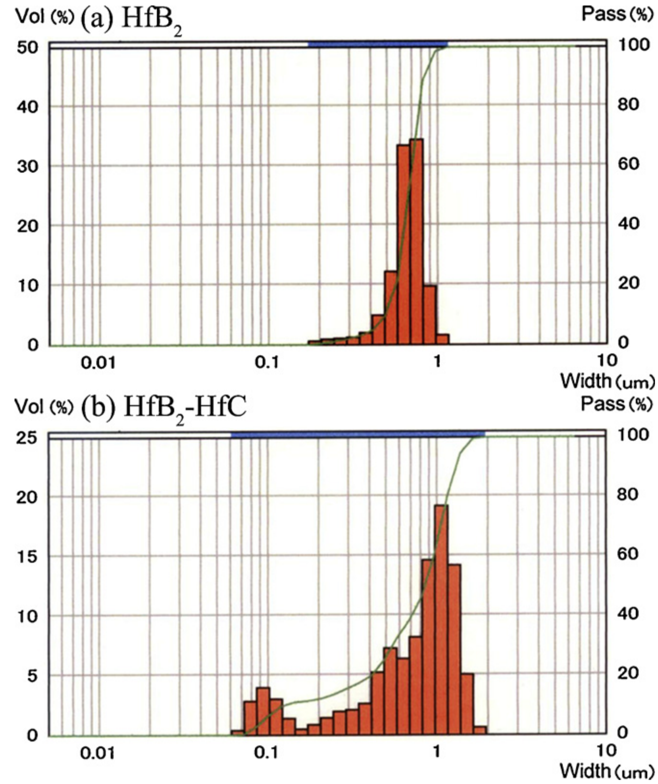

Fig. 3. Particle size distribution of HfB_2 (a) and HfB_2–HfC (b) powders synthesized at 1600 °C.

Fig. 2 shows the SEM micrographs of the as-synthesized HfB_2 and HfB_2–HfC. It is clear that the diameter of HfB_2 and HfB_2–HfC powders distributes from sub-micrometer to micrometer. It also can be found that the synthesized powders show quasi-column morphology with some extent of agglomeration and it is hardly to identify HfB_2 and HfC from their morphology. However, it is easy to see that there is some smaller particles distributed in HfB_2–HfC powders, EDS showed that these small particles were HfC (not shown here). As shown in Fig. 3, the mean diameter of the as-synthesized HfB_2 and HfB_2–HfC powders were presented by laser particle size analysis. Monolithic HfB_2 had a very narrow particle size distribution

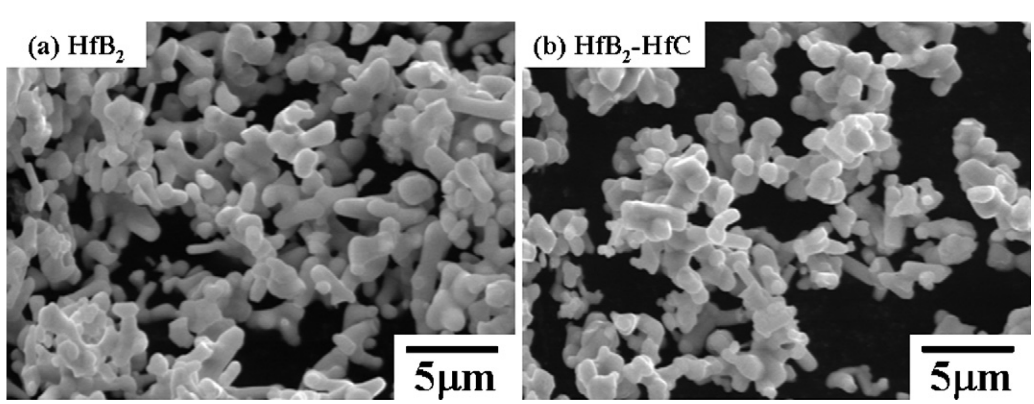

Fig. 2. SEM micrographs of the as-synthesized HfB_2 (a) and HfB_2–HfC (b) powders at 1600 °C for 1 h.

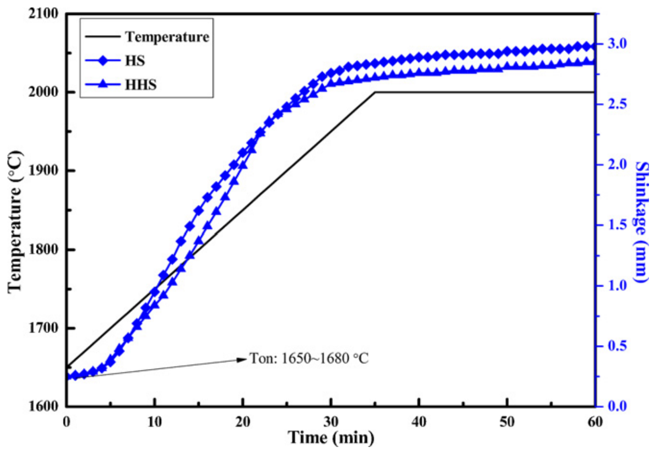

Fig. 4. Shrinkage behavior and temperature profile of HS and HHS composites.

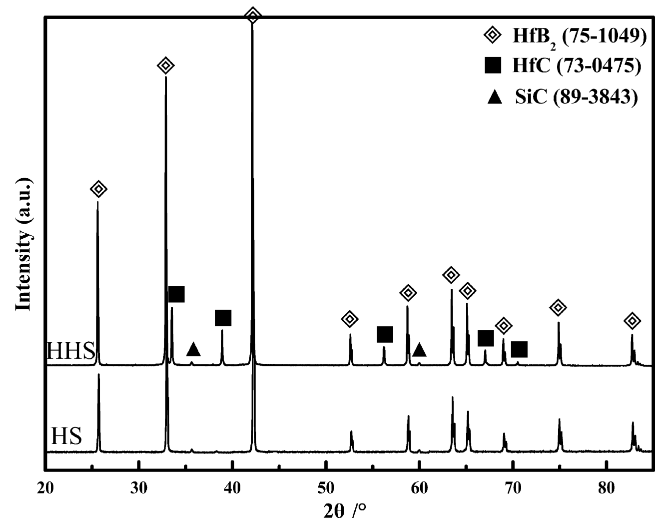

Fig. 5. XRD patterns of hot pressed HS and HHS ceramics.

and its mean diameter was determined about 0.66 μm. However, the particle size of HfB_2–HfC distributed in two regions. The smaller particle size was about 0.1 μm, which was corresponding to HfC. And the larger one was about 1.12 μm, which was corresponding to HfB_2. The small particle size of HfC could ascribe to its low content. As is known, grain growth was associated with mass transfer. And mass transfer process between HfC particles should mainly completed via surface diffusion. Therefore, the low content of HfC reduced the chance of particle contact and hindered grain growth. The particle size of HfB_2 determined by laser particle size analysis seemed a little different from the SEM images (Fig. 2). As is known, laser particle size analysis could be influenced by a lot of factors, especially the dispersion, agglomeration and the particles' shape, etc. In our case, the HfB_2 particles showed quasi-column morphology with some extent of agglomeration, which was likely to result in a certain degree of "distortion" of the determined particle size by laser particle size analysis. Therefore, it was much more reliable to combine with the SEM images to evaluate the particle size.

3.2. Densification, microstructure and mechanical properties of the hot-pressed HS and HHS ceramics

3.2.1. Densification behavior

HS started shrinking at 1650 °C (Fig. 4) and required a maximum temperature of 2000 °C to achieve a nearly full density with a dwell time of 1 h. Its final bulk density was 9.47 g cm^{-3}, corresponding to 98.6% of its theoretical density. For HHS, the mixture started shrinking at 1680 °C and the densification was also completed at 2000 °C with a holding time of about 1 h (Fig. 4). The final bulk density was 9.65 g cm^{-3}, corresponding to 99.2% of its theoretical density. With the incorporation of HfC, the relative densities of HfB_2–SiC ceramics increased from 98.6% to 99.2%, which indicated that HfC could promote the densification of HfB_2–SiC ceramics to some extent. It is considered that the following two factors might relate to the densification promotion of HfC. Firstly, the incorporation of HfC remarkably inhibited the grain growth (as shown in the next part), which administered to the densification process of HfB_2–HfC–SiC ceramics. On the other hand, it is known that oxygen contamination is very harmful to the densification of MB_2-based ceramics. Therefore, the remove of oxygen contamination can promote the densification of MB_2-based ceramics. As shown in the above section, the oxygen content of HfB_2–HfC (0.19 wt%) was lower than HfB_2 (0.30 wt%). At the same time, the small quantity of residual carbon or boron carbide in HfB_2–HfC was helpful to remove the residual oxygen contaminate.[1] Consequently, the above factors resulted in the improved densification of HHS ceramics. The shrinkage behavior of HS and HHS was very similar and their rapid densification process occurred in the temperature range 1750–1950 °C. After dwelling at 2000 °C for 1 h, the shrinkage of HS and HHS could be negligible.

3.2.2. Phase composition and microstructure

As shown in Fig. 5, the hot pressed HS ceramic was composed of hexagonal HfB_2 and SiC, while HHS ceramic was composed of hexagonal HfB_2, SiC and cubic HfC. Therefore, the phase compositions of hot pressed HS and HHS ceramics were consistent with the designed compositions. From the XRD patterns, we can also learn that there is no reaction occurred during hot pressing, which was agreed with the above analysis.

The SEM images of HS and HHS ceramics are shown in Fig. 6, and the measured average grain sizes are summarized in Table 1. As inspected by SEM, both of the ceramic bulks did not reveal any residual porosity, which congruently agreed with their final relative density of higher than 98.5%. Resulting from the low content of oxygen impurity and other impurities of the as-synthesized powders, grain boundaries in both HS and HHS were very clean. At the same time, it could be found that every phase appeared well distributed throughout the samples. In HS ceramics, HfB_2 grains (gray phase) grew up to around 3.14 μm, and some SiC grains (black phase) became elongated, with an average grain size of about 1.25 μm. Compared with the starting HfB_2 and SiC particles, the grains in HS ceramics coarsened markedly. In HHS ceramics, EDS analysis indicated that the gray-white phase was HfC. The average grain size of HfB_2 was approximately 2.07 μm, the SiC grain size

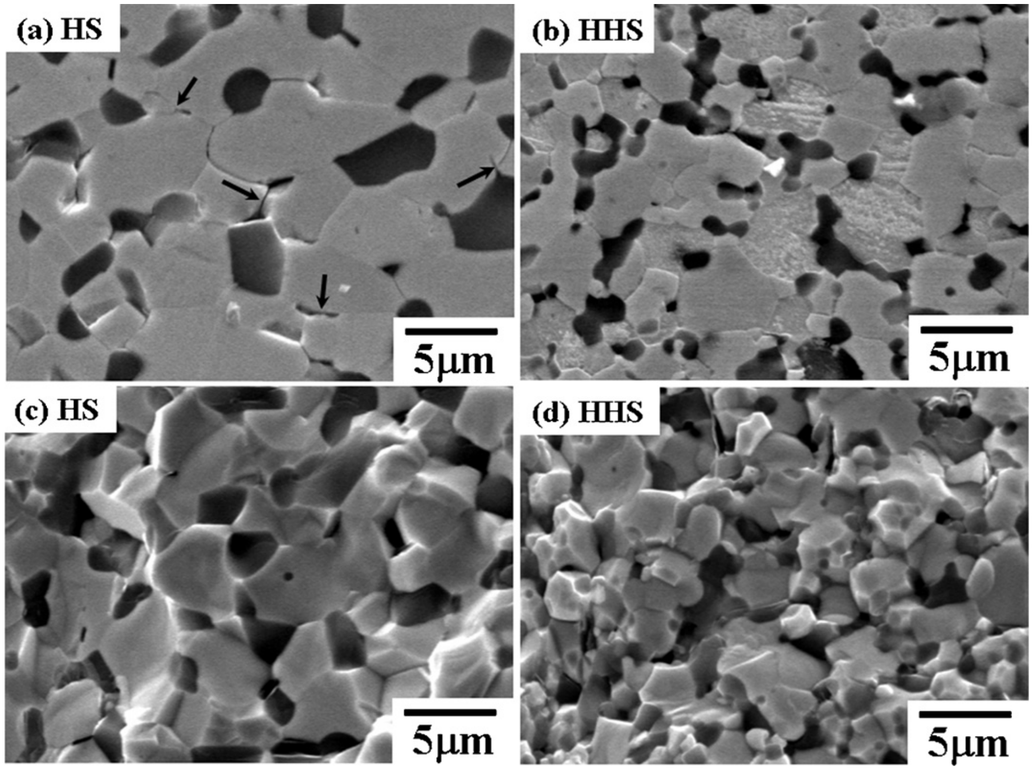

Fig. 6. SEM images of polished and fracture surfaces of hot pressed HS (a and c) and HHS (b and d) ceramics.

was about 0.69 μm and the HfC grain size was about 0.4 μm. The incorporation of HfC remarkably inhibited the grain growth. However, the content of HfC seemed far less than the designed composition (8 vol%). It is considered that composition contrast might relate to this phenomenon. The composition contrast between HfB_2 and HfC is very limited, which becomes negligible under secondary electron image mode. This phenomenon was also observed in Monteverde's results.[8]

In addition, it could be observed that some microcracking at HfB_2/HfB_2 and HfB_2/SiC interfaces presented in HS ceramics (indicated by arrows in Fig. 6(a)). Analogous microcracking phenomenon was also reported by Monteverde in HfB_2–SiC ceramic as well as Guo et al. in ZrB_2–SiC ceramic.[6,8] According to their argument, microcracking was attributed to the emergence of high residual stresses, which appeared at the grain boundaries as a consequence of the mismatch of thermal expansion. Previous studies have widely shown that thermal residual stresses could be developed during cooling from the processing temperature owing to mismatch of thermal expansion.[14] In HfB_2–SiC system, the thermal expansion coefficient of HfB_2 and SiC is $6.3 \times 10^{-6}\,K^{-1}$ and $4.7 \times 10^{-6}\,K^{-1}$. Under the experimental condition in this work, a residual stress as high as ∼1.24 GPa[13] could be developed due to the mismatch of thermal expansion between HfB_2 and SiC, which resulted in the microcracking phenomenon as shown in Fig. 6(a). However, no microcracking was observed in HHS ceramic, which could be ascribed to its fine grain size. Early results have revealed that the development of residual stresses was strongly related to the grain size.[15] Microcracking did not occur in fine-grained materials, while some cracks appeared when the grains reached a certain critical size.[14] Therefore, it could be concluded that the incorporation of HfC eliminated microcracking and stabilized the microstructures.

Table 1
Measured grain size, densities and mechanical properties of hot pressed HS and HHS ceramics.

Properties		HS	HHS
Grain size (μm)	HfB_2	3.14	2.07
	SiC	1.25	0.69
	HfC	–	0.4
True density ($g\,cm^{-3}$)		9.47	9.65
Apparent porosity (%)		0.11	0.09
Relative density (%)		98.6	99.2
Hv5 (GPa)		21.1	19.6
E (GPa)		489.6	499.2
K_{IC} ($MPa\,m^{1/2}$)		3.95	5.09
σ (MPa)		654	863

Actually, microcrack can weaken grain boundary, increase the possibility of intergranular fracture and energy dissipation mechanism to some extent. However, the microcrack density in HS is not very high. Resulting from its large grain size and high strength for grain boundaries, the fracture mode of HS was predominant transgranular and nearly no intergranular fracture was observed (Fig. 6(c)) even if there's some microcrack existing. As shown in Fig. 6(d), the dominant fracture mode of HHS composite was transgranular as well. However, a certain amount of intergranular behavior was also observed in HHS, partly due to

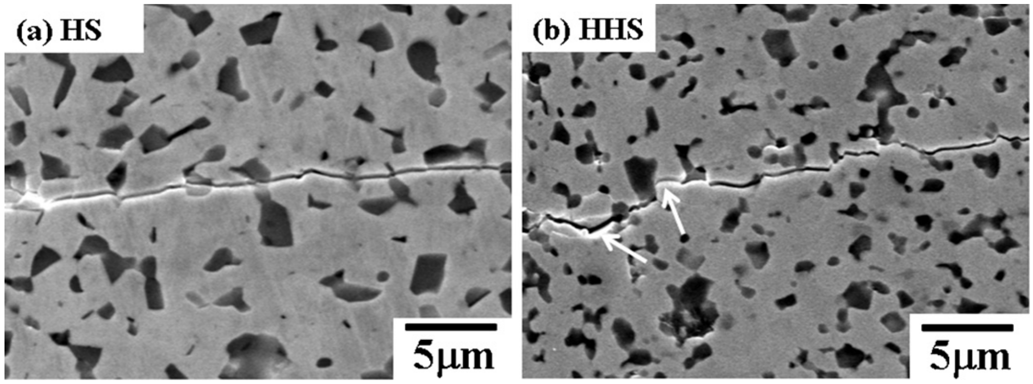

Fig. 7. SEM images of indentation crack propagation of hot pressed HS (a) and HHS (b) ceramics.

its fine grain size. This implied that HHS might have relatively higher fracture toughness than HS.

3.2.3. Mechanical properties

The tested values of the mechanical properties are summarized in Table 1. The Vickers' hardness of HS ceramic was 21.1 GPa, which is consistent with the reported values (19–21 GPa) for HfB_2–20 vol% SiC by Marschall et al.[16] and Gasch et al.[17] With the incorporation of HfC, the Vickers' hardness of HHS decreased to 19.6 GPa, which is close to the value of reactive hot pressed HfB_2–HfC–SiC composite reported by Monteverde.[8] In ZrB_2–ZrC–SiC system, the addition of ZrC usually increases the hardness of ZrB_2–SiC ceramics partly due to the higher hardness of ZrC than ZrB_2.[6] However, the intrinsic hardness of HfC (29 GPa) and HfB_2 (28 GPa) is very close,[18] the incorporation of HfC to HfB_2–SiC system usually result in the decrease of hardness, which has also been reported by Licheri et al. in spark plasma sintered HfB_2–SiC and HfB_2–HfC–SiC composites.[9] Generally, the finer grain size can increase the frequency with which dislocations encounter grain boundaries, thus heightening the amount of stress required for deformation. At a given indent load, less deformation zone and higher hardness could be expected in grain-refined material. However, grain-refined HHS had a lower hardness compared with HS, which seemed object to the above analysis. Therefore, there should be some other factors determining the hardness of HHS. In the future work, we will study further the factors that influence the hardness with the aim of obtaining higher values.

In terms of absolute value, the Young's modulus (E) of HS and HHS ceramics was 489.6 GPa and 499.2 GPa respectively, which agrees well with that reported values for similar compositions.[17] As well, the Young's modulus of HS and HHS are in very good agreement with the calculated values (i.e. 513 GPa and 508 GPa for HS and HHS, respectively) using a rule of mixture,[19] namely the arithmetic average $\Sigma Q_i E_i$, where E_i and Q_i are the Young's modulus and volume fractions of phases constituting the composites. For Young's modulus calculation, the following data of E_i was used: 530 GPa[20] for HfB_2, 460 GPa[21] for HfC, and 448 GPa[18] for SiC.

The fracture toughness for HS ceramic was 3.95 MPa $m^{1/2}$, which was close to the reported value (4.1 MPa $m^{1/2}$) for hot pressed HfB_2–20 vol% SiC ceramic fabricated using commercial HfB_2 powder by Gasch et al.,[17] but much lower than the reported value (6.29 MPa $m^{1/2}$) of hot pressed HfB_2–20 vol% SiC ceramic based on HfB_2 powder synthesized by borothermal reduction of HfO_2 in our previous work.[13] With the incorporation of HfC, the fracture toughness for HHS ceramic increased to 5.09 MPa $m^{1/2}$, which was 29% higher than HS. As shown in Fig. 7, the Vickers-indentation induced crack propagation path on polished surfaces of HS and HHS ceramics were observed by SEM, where we can get some useful information to discuss their toughening mechanisms. As the predominant fracture mode of HS was transgranular, crack deflection appeared neglectable in the crack propagation path (Fig. 7(a)). However, the indentation crack path in HHS ceramics seems much more tortuous. Crack deflection and bridging (indicated by arrows in Fig. 7(b)) increased energy dissipation during crack propagation, resulting in higher fracture toughness for HHS ceramic.

The flexural strength of HS and HHS ceramics were 654 MPa and 863 MPa respectively. With the incorporation of HfC, the bending strength of HHS ceramics increased significantly. Previous studies have shown that grain size was a critical factor determining the strength of MB_2–SiC (M = Zr, Hf), and grain growth (especially the grain growth of SiC) would lead to the strength reduction.[22,23] Zhu et al. reported that the bending strength of ZrB_2–SiC decreased from around 909 MPa with SiC grain size of about 1 μm to approximately 389 MPa with SiC grain size of about 6 μm.[23] Therefore, the relatively low strength of HS could mainly ascribe to its larger average grain size, especially SiC. With the incorporation of HfC, the reduction of grain size led to the increase of bending strength. On the other side, according to the Griffith equation, a small flaw size should increase strength[22]:

$$\sigma = \frac{K_{IC}}{Y\sqrt{a}} \quad (7)$$

where σ is the flexural strength of the material, K_{IC} is the fracture toughness, Y is a geometric constant, and a is the critical flaw size in the material. According to fracture mechanics, the strength and, thus, the reliability of ceramics are governed by detrimental flaws, one of which behaves as a fracture origin. A wide variety of features is known to behave as detrimental structures, such destructive cracks, pores and coarse particles.

Benefitting from the relative densities higher than 98.5%, no visible residual porosity was detected from SEM images for both HS and HHS (Fig. 6(a) and (b)). As well, no abnormal coarse particles or inclusions were detected from SEM images. Detailed analysis of the tensile fracture surfaces of HS and HHS in bending test showed similar morphology to Fig. 6(c) and (d), respectively. No destructive large defects were identified in the fracture origins. Therefore, the critical flaw size could be preliminarily regarded as the characteristic grain size of HS and HHS. Besides, fracture toughness is also an important factor for flaw tolerance. Therefore, the high fracture toughness of HHS is also an important factor contributed to its high bending strength.

4. Conclusion

In this work, we mainly investigated the influence of HfC on the microstructure and properties of HfB_2–SiC system. Firstly, HfB_2 and HfB_2–10 vol% HfC powders were synthesized by carbo/borothermal reduction. Then, HfB_2–20 vol% SiC (HS) and HfB_2–8 vol% HfC–20 vol% SiC (HHS) ceramics were hot pressed using as-synthesized HfB_2, HfB_2–10 vol% HfC and commercially available SiC as starting powders. Analysis indicated that the incorporation of HfC promoted the densification and fined the microstructure of HfB_2–SiC ceramics. With the incorporation of HfC, the fracture toughness and flexural strength of HHS (5.09 MPa $m^{1/2}$, 863 MPa, respectively) were much higher than HS (3.95 MPa $m^{1/2}$, 654 MPa, respectively); the elastic modulus of HHS (499.2 GPa) and HS ceramics was similar (489.6 GPa), while the hardness of HHS (19.6 GPa) was a little lower than HS (21.1 GPa).

Acknowledgments

Financial supports from the Chinese Academy of Sciences under the Program for Recruiting Outstanding Overseas Chinese (Hundred Talents Program), the National Natural Science Foundation of China (No. 50632070), the Science and Technology Commission of Shanghai (No. 08520707800 and No. 09ZR1435500), and the CAS Special Grant for Postgraduate Research, Innovation and Practice are greatly appreciated.

References

1. Fahrenholtz WG, Hilmas GE, Talmy IG, Zaykoski JA. Refractory diborides of zirconium and hafnium. *J Am Ceram Soc* 2007;**90**:1347–64.
2. Medri V, Monteverde F, Balbo A, Bellosi A. Comparison of ZrB_2–ZrC–SiC composites fabricated by spark plasma sintering and hot-pressing. *Adv Eng Mater* 2005;**7**:159–63.
3. Bellosi A, Monteverde F, Sciti D. Fast densification of ultra-high-temperature ceramics by spark plasma sintering. *Int J Appl Ceram Technol* 2006;**3**:32–40.
4. Wu WW, Zhang GJ, Kan YM, Wang PL. Reactive hot pressing of ZrB_2–SiC–ZrC ultra high-temperature ceramics at 1800 °C. *J Am Ceram Soc* 2006;**89**:2967–9.
5. Licheri R, Qrru R, Musa C, Cao G. Combination of SHS and SPS techniques for fabrication of fully dense ZrB_2–ZrC–SiC composites. *Mater Lett* 2008;**62**:432–5.
6. Guo WM, Zhang GJ. Microstructures and mechanical properties of hot-pressed ZrB_2-based ceramics from synthesized ZrB_2 and ZrB_2–ZrC powders. *Adv Eng Mater* 2009;**11**:206–10.
7. Bull J, White MJ, Kaufman L. Ablation resistant zirconium and hafnium ceramics for space vehicles-comprise zirconium diboride, zirconium carbide, and silicon carbide, or hafnium diboride, hafnium carbide, and silicon carbide or other combinations of these materials. US Patent 5750450-A 1998-296791 [30].
8. Monteverde F. Progress in the fabrication of ultra-high-temperature ceramics: in situ synthesis, microstructure and properties of a reactive hot-pressed HfB_2–SiC composite. *Compos Sci Technol* 2005;**65**:1869–79.
9. Licheri R, Orru R, Musa C, Locci AM, Cao G. Consolidation via spark plasma sintering of HfB_2/SiC and HfB_2/HfC/SiC composite powders obtained by self-propagating high-temperature synthesis. *J Alloys Compd* 2009;**478**:572–8.
10. Ni DW, Zhang GJ, Kan YM, Wang PL. Synthesis of monodispersed fine hafnium diboride powders using carbo/borothermal reduction of hafnium dioxide. *J Am Ceram Soc* 2008;**91**:2709–912.
11. Liu YH, Liu PA. *X-ray diffraction analysis theoretics and application*. China: Chemical Industry Press; 2003. p. 127–34.
12. Evans AG, Charles EA. Fracture toughness determinations by indentation. *J Am Ceram Soc* 1976;**59**:371–2.
13. Ni DW, Zhang GJ, Kan YM, Wang PL. Hot pressed HfB_2 and HfB_2–20 vol% SiC ceramics based on HfB_2 powder synthesized by borothermal reduction of HfO_2. *Int J Appl Ceram Technol* 2010;**7**:830–6.
14. Tvergaard V, Hutchinson JW. Microcracking in ceramics induced by thermal-expansion or elastic-anisotropy. *J Am Ceram Soc* 1988;**71**:157–66.
15. Rice RW, Freiman SW, Becher PF. Grain-size dependence of fracture energy in ceramics. 1. Experiment. *J Am Ceram Soc* 1981;**64**:345–50.
16. Marschall J, Erlich DC, Manning H, Duppler W, Ellerby D, Gasch M. Microhardness and high-velocity impact resistance of HfB_2/SiC and ZrB_2/SiC composites. *J Mater Sci* 2004;**39**:5959–68.
17. Gasch M, Ellerby D, Irby E, Beckman S, Gusman M, Johnson S. Processing, properties and arc-jet oxidation of hafnium diboride/silicon carbide ultra high temperature ceramics. *J Mater Sci* 2004;**39**:5925–37.
18. Smith ER, Johnson D, Brockway CM, Thompson JK. *Engineering property data on selected ceramics*, vol. II. Columbus, OH: Carbides, Metals and Ceramics Information Center, Battelle, Columbus Laboratories; 1979.
19. Torquato S. Modelling of physical properties of composites materials. *Int J Solids Struct* 2000;**37**:411–22.
20. Kotelnikov RB, Bashlykov SN, Galiakbarov ZG, Kashtanov AI. *Handbook of high melting point materials*. Moscow: Metallgiya Press; 1969.
21. Brown HL, Armstrong PE, Kempter CP. Elastic properties of some polycrystalline transition-metal monocarbides. *J Chem Phys* 1966;**45**:547–9.
22. Rezaie A, Fahrenholtz WG, Hilmas GE. Effect of hot pressing time and temperature on the microstructure and mechanical properties of ZrB_2–SiC. *J Mater Sci* 2007;**42**:2735–44.
23. Zhu SM, Fahrenholtz WG, Hilmas GE. Influence of silicon carbide particle size on the microstructure and mechanical properties of zirconium diboride–silicon carbide ceramics. *J Eur Ceram Soc* 2007;**27**:2077–83.